Received 16 March 2023; revised 16 April 2023; accepted 21 April 2023. Date of publication 1 May 2023; date of current version 15 June 2023.

Digital Object Identifier 10.1109/OJCOMS.2023.3272219

Introduction to Mediumband Wireless Communication

DUSHYANTHA A. BASNAYAKA (Senior Member, IEEE)

School of Electronics Engineering, Dublin City University, Dublin 9, Ireland

CORRESPONDING AUTHOR: D. A. BASNAYAKA (e-mail: d.basnayaka@dcu.ie)

This work was presented in part at IEEE Vehicular Technology Conference (VTC-Fall) held in London–Beijing, September 2022 [DOI: 10.1109/VTC2022-Fall57202.2022.10012908].

ABSTRACT The multipath is unavoidable in radio frequency (RF) wireless communication, and affects almost every element of the communication systems. The impact of multipath on the received signal depends on whether the delay spread (i.e., spread of time delays associated with different multipath components) is large or small relative to the symbol period of the wireless communication system. In narrowband channels, the symbol period is set such that the delay spread is about one tenth (or less) of it. In broadband channels, it is set such that the delay spread is many times greater than the symbol period. In between these two extremes, there appears to exist an important, yet overlooked, class of channels whose delay spread is neither small nor large enough for them to fall into these two basic channel classes. In this paper, we study the effect of multipath on channels that fall in the transitional region between narrowband and broadband referred henceforth as "***mediumband***". This paper shows that mediumband channels possess a distinct channel model, and pose both challenges and opportunities for reliable wireless communication. For instance, mediumband channels enable signalling at a significantly higher rate than that of narrowband channels, but on the flip side, as the degree of mediumband-ness increases, the quality of the channel deteriorates rapidly due to the excessive inter-symbol-interference (ISI). However, mediumband channels have an inherent ability to avoid deep fading, and if designed properly, mediumband wireless communication, which refers to wireless communication through mediumband channels, could be made to be significantly more reliable too.

INDEX TERMS Communication theory, multipath, delay spread, wireless channel models.

I. INTRODUCTION

WIRELESS communication is indispensable to the modern living, and is one of the main driving forces of the ongoing digital transformation [1]. Its ability especially to keep people connected on-the-go and in emergencies are particularly appealing. Today, not only people, but devices also have the ability to communicate wirelessly, and the number of devices that require wireless connectivity is exponentially growing [2]. It has been predicted that the number of such devices will grow to over 13 billion by the end of 2023 [3]. In order to enable wireless communication for such a large number of devices cost-effectively and sustainably, simple and cost-effective physical layer wireless communication technologies are required. Furthermore, these devises may have different requirements in terms of spectral efficiency, reliability, energy efficiency and security [4]. So, having a spectrum of physical layer wireless communication technologies is more important than ever.

In modern digital radio wireless communication, the transmitter (TX) sends information by transmitting a modulated electromagnetic (EM) wave, where typically the envelope of the EM wave varies according to an information signal. This information signal is typically an analog signal, but in digital wireless radio communication, only the signal points separated regularly in time carry useful information. This separation distance in time, which is an important parameter, is known as the symbol period (say T_s) [5].

The wireless propagation environment between the TX and the receiver (RX) plays an important role too. It typically comprises of natural, man-made, and moving & static objects. EM wave emanating from the TX spreads out

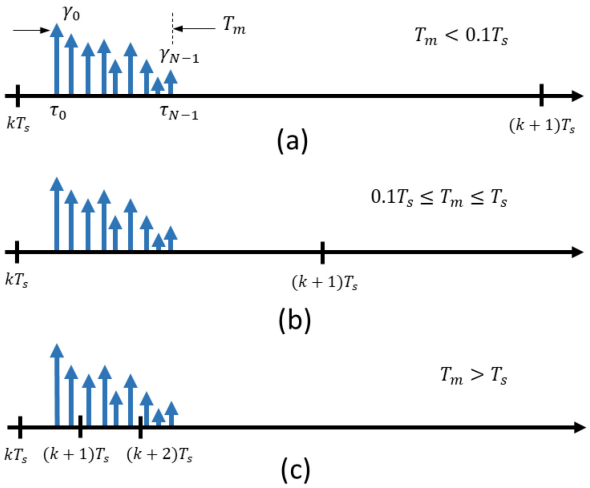

FIGURE 1. A depiction of a typical multipath profile of a) a narrowband channel, b) a mediumband channel, and c) a broadband channel, where the delay spread T_m is the same in all cases. The horizontal excess delay axis is divided into time bins of duration T_s, which is the symbol period of the baseband equivalent data signal. This T_s has nothing to do with the wireless propagation environment. For the same multipath profile, depending on T_s in comparison with T_m, a channel fall into the narrowband, mediumband or broadband regime.

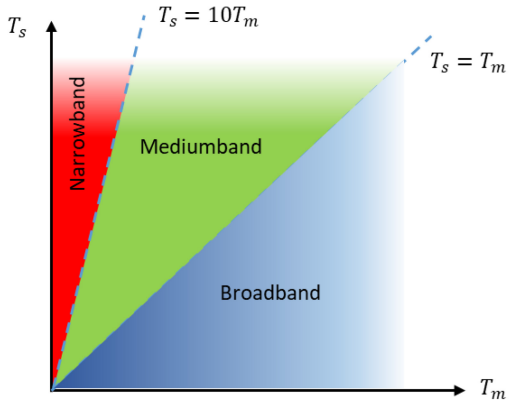

FIGURE 2. Three main regions on $T_m T_s$–plane along with the designated channel models. Theoretically, there is no restriction on the use of a non-designated channel model in these regions, but such uses are not typical, and may be physically less meaningful and unnecessary.

spatially as it travels through the space drastically reducing its strength per unit space. This phenomenon gives rise to an effect commonly known as path loss in wireless communication [6]. Also, the transmitted EM wave undergoes reflections and diffractions before being received by the RX [5]. The combine effect of these affects the received signal at the RX, and in turn the wireless communication profoundly [8].

The RX receives an untidy mixture of attenuated and delayed versions (i.e., multipath) of the transmitted signal before the received signal being sampled and decoded [9], [10]. In the absence of a line-of-sight (LoS) between the TX and the RX, which is the case in overwhelming number of instances of daily communications between people, it is often this multipath that enables wireless communication. On the other hand, in the presence of severe multipath, it is a considerably involving task to effectively and reliably detect the desired signal. Over 60 years of wireless communication research efforts have been, and also are being, dedicated to perfect the art of detection of the desired signal from this untidy mixture of signals [5], [7]. The current state-of-the-art in wireless communication is 5th-generation (5G) [11], [12].

The distribution of multipath may be depicted as an impulse train as shown in Fig. 1, where the relative strength of the multipath components are represented by the height, and the relative delays are represented by the horizontal separation distance of these impulses. The strengths and delays of multipath components are highly environment-dependent, hence random, but typically the strength reduces as the delay increases. One of the most important quantities of interest is the delay spread (say T_m), which effectively is the delay between the latest and the earliest significant multipath components. Considering a random wireless propagation environment with a certain delay spread, this paper asks how exactly multipath affects wireless communication, and what are the ways to harness the benefits of multipath for wireless communication?

Modern digital wireless communication uses different channel models, primarily "*narrowband*" and "*broadband*" to capture the essence of different multipath scenarios [13], [17]. The effect of multipath, especially the relative strengths and delays, appears in different ways, often as fading factors, in these channel models. It is those models that form the foundation of all the key functions of today's digital wireless communication systems. Those models are used for channel estimation algorithms [18], interference management [19], [20], capacity studies [21], and also to develop innovative transceiver techniques [20], [22]. The performance of wireless communication systems is largely determined by how accurately channel models capture the underlying propagation scenarios, and also by the condition (e.g., strength and the statistics) of the fading factors that arise in the channel models [17], [23], [24], [25].

A. NARROWBAND VS BROADBAND

Narrowband: A wireless channel is said to be narrowband (or frequency-nonselective), if the symbol period T_s is set such that it is significantly greater than the delay spread T_m. As shown in Fig. 2, typically the narrowband condition is deemed to be satisfied if [27]:

$$T_m < 0.1T_s. \tag{1}$$

In this regime, the TX should reduce the symbol rate[1] significantly in order at least to ensure (1). A lower symbol rate means a lower data rate, which is typically undesirable. In narrowband channels, the effect of multipath reduces to a single multiplicative fading factor. Hence the multipath is said to be nonresolvable. After estimating this fading factor, simpler single-user detection can be applied for information detection [17].

1. In digital wireless communication, symbol rate is equal to $1/T_s$.

Broadband: A wireless channel is said to be broadband (or frequency-selective) if:

$$T_s < T_m. \tag{2}$$

This typically leads to a tapped delay line channel model with as many taps as $\lceil T_m/T_s \rceil$, where $\lceil . \rceil$ denotes the ceiling operation [28]. The strength of these taps are dependent on the path gains and relative delays of multipath components [29], [30], [31], [32]. For instance, if $T_m \approx 1.2T_s$, the effect of multipath is often modelled with two fading factors (i.e., taps). Hence, the multipath is said to be resolved up to some extent. Using these tap weights as the basis, multi-carrier modulation schemes like SC-FDM (single-carrier-frequency-division-multiplexing) or OFDM (orthogonal-frequency-division-multiplexing) for wireless communication over broadband channels are often designed [27, p. 386]. The broadband systems can achieve significantly higher data rates, but at the cost of significantly higher signal processing overhead and energy consumption. Falling between these two extremes are mediumband channels [34].

B. MEDIUMBAND

Wireless communication systems could encounter scenarios, either intermittently or otherwise, where the delay spread satisfies neither the narrowband condition that is (1) nor the broadband condition, which is (2). For instance, in the transitional region [34][2]:

$$T_m \leq T_s \leq 10T_m, \tag{3}$$

which is in GREEN in Fig. 2, the effect of multipath cannot be simply reduced to a single multiplicative fading factor, but the delay spread is not sufficiently wide enough (with respect to T_s) to add further taps to resolve multipath either. This paper considers this transitional region defined by (3), and studies how the effect of multipath can be accurately captured in a channel model for the class of radio frequency wireless channels that fall in this region referred henceforth as "***mediumband***". Furthermore, how the effect of mediumband-ness affects the key aspects of wireless systems such as I/Q processing and information detection is also studied.

Depending on the relative strength of T_m in comparison with T_s, the degree of mediumband-ness of mediumband channels varies. A simple metric like percentage delay spread (PDS) defined by:

$$\text{Percentage Delay Spread (PDS)} = \left(\frac{T_m}{T_s}\right) \text{ x } 100\%, \tag{4}$$

may be used to capture this degree of mediumband-ness of mediumband channels as a percentage. It is straightforward that, in the mediumband region, the corresponding PDS is $10\% \leq \text{PDS} \leq 100\%$.

In this paper, the effect of multipath on mediumband channels has been shown to be two-fold. As in the narrowband case, the effect of multipath appears as a multiplicative fading factor for the desired signal. The multipath also gives rise to an additive interference, which is a form of inter-symbol-interference (ISI). It has also been shown that this ISI increases as the degree of mediumband-ness increases (see Fig. 5).

Extending the main analysis for the original mediumband channels, this paper further analyses what we call "***generalized mediumband channels***" that typically exist in the transitional regions between broadband channels of L taps and $L+1$ taps, where $L = 2, 3, \ldots$

C. WHY THE STUDY OF MEDIUMBAND WIRELESS COMMUNICATION MATTERS?

The study of mediumband channels (and also the mediumband wireless communication) has two main objectives. The mediumband channels could occur intermittently or permanently. Hence, firstly, it enables the quantitative analysis of the effects of mediumband-ness that could intermittently arise in conventional channels. Secondly, as shown in Section IV, since the symbol period can be made to be smaller than that of narrowband systems, the signalling can be done at a higher rate in mediumband systems enabling significantly higher data rate than that of narrowband systems. On the flip side, as the signalling rate increases, otherwise as the degree of mediumband-ness increases, ISI increases and in turn, the quality of the channel decreases rapidly. However, the fading factors arisen in mediumband channels exhibit favorable statistical properties for wireless communication such as "***deep fading avoidance***". This deep fading avoidance effect is such that it can significantly mitigate the unfavourable effects of ISI in all practically relevant signal-to-noise ratio (SNR) regions, as can be seen in the gains of bit error rate (BER) performance even with simple single-user detection, which is about several dBs. Therefore, operating in the mediumband region is not a sacrifice of reliability for higher data rates, but if designed properly, can be made to be a "***win − win***" situation. More detail on the wider implications of this work can also be found in Section VIII.

The organization of the rest of the paper is as follows. Section II elaborates the wireless propagation environment considered in this paper, and Section III presents a channel characterization for mediumband channels. Sections IV–VI discuss the aspects of signal-to-interference-ratio, I/Q processing, and information detection of mediumband channels respectively. In Section VII, the notion of generalized mediumband channels is introduced and analysed, and in Section IX, conclusions are drawn.

II. PROPAGATION ENVIRONMENT

A radio wave (RF) wireless communication system with a single TX and a single RX in a rich scattering environment as

2. The boundary equations, (1), (2) and (3) are for indicative purposes only. There is no restriction on the use of one channel model for another region on T_mT_s–plane. The use of a particular channel model for a certain wireless communication scenario, or region on T_mT_s–plane, is dependent on many factors like the required level of reliability and the affordable complexity.

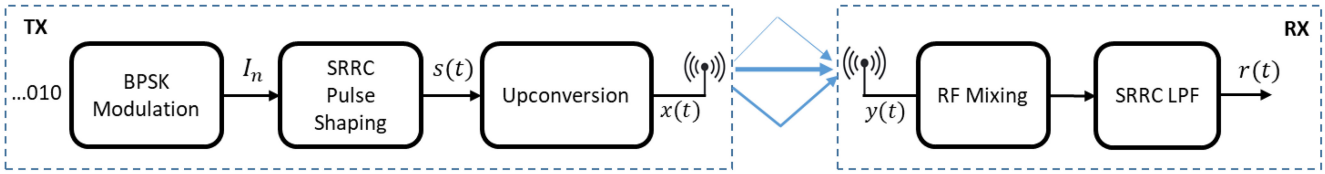

FIGURE 3. A simplified schematic diagram of a typical radio wave communication system, where only the key subsystems are shown.

shown in Fig. 3 is considered [27]. Let $s(t)$ be the baseband equivalent transmitted signal corresponding to a single frame:

$$s(t) = \sum_k I_k g(t - kT_s), \tag{5}$$

where T_s is the symbol period, $\{I_k\}$ is the sequence of amplitudes drawn from a 2^b element constellation (e.g., BPSK, 4-PAM, 4-QAM, etc.) by mapping b-bit binary blocks from an underlying information sequence d_k, and $g(t)$ is the pulse shaping filter. Combining the effects of square-root-raised-cosine (SRRC) transmit and receive pulse shaping filters, we herein assume a raised-cosine pulse for $g(t)$ with a roll-off factor β. So, $g(t)$ in the time domain is given by [5, eq. 4.49]:

$$g(t) = \begin{cases} \frac{\pi}{4}\text{sinc}\left(\frac{1}{2\beta}\right), & t \pm \frac{T_s}{2\beta} \\ \text{sinc}\left(\frac{t}{T_s}\right)\frac{\cos\left(\frac{\pi\beta t}{T_s}\right)}{1-\left(\frac{2\beta t}{T_s}\right)^2}, & \text{otherwise.} \end{cases} \tag{6}$$

In this paper, solely for simplicity, we assume only one dimensional constellations like BPSK, 4-PAM resulting in real amplitudes, which in turn ensures that, $s(t)$ is real. The transmitted RF signal is mathematically given by:

$$x(t) = \text{Re}\left\{\sqrt{E_s}s(t)e^{j2\pi F_c t}\right\}, \tag{7}$$

where F_c is the carrier frequency, and E_s is a factor that controls the transmit power. It is also assumed that the sequence $\{I_k\}$ is normalized such that $\mathcal{E}\{|I_k|^2\} = 1$, which due to the effect of the raised-cosine pulse in turn gives:

$$\mathcal{E}\left\{|s(t)|^2\right\} = 1 - 0.25\beta. \tag{8}$$

Also (7) ensures that $\mathcal{E}\{|x(t)|^2\} = 0.5E_s(1 - 0.25\beta)$. The received RF signal at the RX, $y(t)$, can be given as a sum of multipath components as:

$$y(t) = \sqrt{E_s}\sum_{n=0}^{N-1} \text{Re}\left\{\alpha_n s(t - \tau_n)e^{j2\pi F_c(t-\tau_n)}\right\}, \tag{9}$$

where N is the number of multipath components, and τ_n and α_n are the absolute time delay and the path gain of the nth component respectively. In the absence of the noise, the received baseband equivalent signal, $r(t)$, can be given by [5]:

$$\begin{aligned} r(t) &= \sqrt{E_s}\sum_{n=0}^{N-1} \alpha_n e^{-j2\pi F_c\tau_n}s(t - \tau_n), \\ &= \sqrt{E_s}\sum_{n=0}^{N-1} \alpha_n e^{-j\phi_n}s(t - \tau_n), \end{aligned} \tag{10}$$

where $\phi_n = 2\pi F_c\tau_n$ is known as the phase of the nth component. It is assumed that, the propagation parameters α_n, τ_n and ϕ_n are constant at least within the time duration of a single frame corresponding to the case of static terminals or terminals with slow relative movement.[3] Without loss of generality, 0 is assumed to be the index of the earliest path meaning α_0 and τ_0 are respectively the path gain and the absolute delay of the earliest (also the shortest) path. Let the delay spread be defined by [13]:

$$T_m = \max_n |\tau_n - \tau_0|. \tag{11}$$

When T_m and T_s fall into different regions on the T_mT_s–plane (see Fig. 2), this paper asks how $r(t)$ can be accurately captured in a channel model, and how the wireless propagation parameters α_ns, ϕ_ns, and τ_ns affect the different fading factors arisen in those channel models, especially the mediumband. Also, how accurately these models fit the underlying $r(t)$ and what is the strength of model mismatch errors, if any, are among the questions that this paper aims to settle.

A. COMPUTER SIMULATION ENVIRONMENT

In order to assess the performance of the proposed mediumband channel model, and also to compare them with other channel models, the generic propagation model described in (10) is simulated on MATLAB. Typically τ_ns are dependent on the environment, but without loss of generality, we assume $\tau_0 = 0$. The other delays τ_n for $n = 1, \ldots, N-1$ are drawn from a uniform distribution, $U[0, T_m]$, where T_m is the delay spread [35]. The sequence of amplitudes are drawn from a BPSK constellation, so $\{I_k\} \in \{-1, 1\}$ $\forall k$. Furthermore, the phases are drawn from a uniform distribution, $\phi_n \sim U[0, 2\pi]$, and equal path gains are considered. These assumptions correspond to one of the most severe propagation environments for wireless communication. In order to ensure $\sum\alpha_n^2 = 1$, the path gains are normalized such that $\alpha_1 = \alpha_2 = \cdots = \alpha_n \propto 1/\sqrt{N}$. By changing T_m appropriately while keeping T_s fixed, mediumband channels (and also other narrowband and broadband) with different degrees of mediumband-ness are obtained. Unless otherwise is specified, in all simulations in this paper, $T_s = 1$ is assumed.

III. MEDIUMBAND CHANNEL CHARACTERIZATION

We firstly recall the narrowband channel model. As depicted in Fig. 1-(a), in narrowband channels, the distribution of

3. Note that this assumption means the channels considered in this paper are time-nonselective.

multipath delays is such that the condition (1) is at least approximately satisfied. As a result, the received baseband equivalent signal in (10) reduces to [27]:

$$r(t) \approx \sqrt{E_s}\left(\sum_{n=0}^{N-1}\gamma_n\right)s\big(t-\hat{\tau}\big), \\ = \sqrt{E_s}g_o s\big(t-\hat{\tau}\big) \tag{12}$$

where the complex path gains, $\gamma_n = \alpha_n e^{-j\phi_n}\ \forall n$, and $g_o = \sum_{n=0}^{N-1}\gamma_n$. Here the multipath components are said to be nonresolvable, and combined into a single multipath with delay $\hat{\tau} \approx \tau_0 \cdots \approx \tau_{N-1}$. The symbol timing synchronizer at the RX typically synchronizes to this common delay, $\hat{\tau}$ [27], [33].

As the channel drifts into the mediumband regime, which occurs when $T_m \leq T_s \leq 10T_m$, even though the multipath components are still nonresolvable, the IO relationship in (12) is seen to be no longer accurate. The simulation studies in Section IV show that, as T_m increases beyond $0.1T_s$, the narrowband identity in (12) weakens gradually. Hence, using (12) as the basis, in this section, we derive a new characterization for mediumband channels, which is:

Theorem 1: In the mediumband regime, the baseband equivalent received signal in the absence of the noise can be accurately modelled as:

$$r(t) = \sqrt{E_s}h_o s\big(t-\hat{\tau}\big) + \sqrt{E_s}\eta_o u(t), \tag{13}$$

where $s(t-\hat{\tau})$ is the desired signal; $u(t)$ is a complex uncorrelated zero mean unit variance interference signal; and $\hat{\tau}$ is the time, which the RX synchronizes to. Consequently, the baseband equivalent received signal in the presence of the noise can be given by:

$$r'(t) = r(t) + n(t), \tag{14}$$

where $n(t)$ is a complex zero mean additive-white-Gaussian-noise (AWGN) signal with variance $\sigma^2 = \mathcal{E}\{|n(t)|^2\}$. The fading coefficients h_o and η_o are given respectively by:

$$h_o = \frac{\sum_{n=0}^{N-1}\gamma_n R\big(\tau_n-\hat{\tau}\big)}{1-\frac{\beta}{4}}, \tag{15}$$

and (16), as shown at the bottom of the page, where $R(\tau) = \mathcal{E}\{s(t)s(t+\tau)\}$ is the autocorrelation function of $s(t)$, which is given in (17), as shown at the bottom of the page and graphically shown in Fig. 4. The noise variance σ^2 is not dependent on the propagation parameters, but only dependent on the noise bandwidth of the pulse shaping filter at the RX, and the spectral density of the thermal noise N_0. Collectively, $\sqrt{E_s}\eta_o u(t)$ may be referred as the model mismatch error signal.

Proof: A detailed proof is first reported in [34], but for the completeness, it is also available in the Appendix. ■

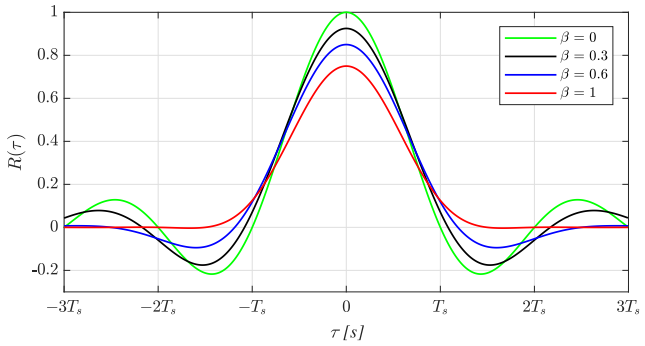

FIGURE 4. $R(\tau)$ for different values of β, where $R(0) = 1 - 0.25\beta$.

The model in (13) and (14) show the desired, interference, and noise signals in additive form, and the effect of multipath is conveniently captured as multiplicative factors. The model also captures the effects of transmit power through E_s, pulse shaping through β, and modulation through $R(\tau)$. In the sequel, a few notable observations about the proposed mediumband channel model are made.

A. NARROWBAND CHANNEL AS A SPECIAL CASE

It can be seen that, the narrowband model in (12) is a special case of the mediumband model in (13). Consider h_o and η_o as $T_m = \max_n|\tau_n - \tau_0| \to 0$. As $T_m \to 0$, all delay deferences (i.e., $\tau_n - \tau_m$ and $\tau_n - \hat{\tau}\ \forall n, m$) also approach zero. Therefore, (17) yields:

$$\lim_{|\tau_n-\hat{\tau}|\to 0} R\big(\tau_n-\hat{\tau}\big) = 1-\frac{\beta}{4}, \qquad \forall n \tag{18a}$$

$$\lim_{|\tau_n-\tau_m|\to 0} R(\tau_n-\tau_m) = 1-\frac{\beta}{4}. \qquad \forall n, m \tag{18b}$$

Substituting these limits into equations for h_o and η_o in (15) and (16) respectively, it can be shown that:

$$\lim_{\substack{|\tau_n-\hat{\tau}|\to 0 \\ \forall n}} h_o = \sum_{n=0}^{N-1}\gamma_n = \sum_{n=0}^{N-1}\alpha_n e^{-j\phi_n}, \tag{19a}$$

$$\lim_{\substack{R(\tau_n-\tau_m)\to\left(1-\frac{\beta}{4}\right) \\ \forall n,m}} \eta_o = 0, \tag{19b}$$

which ensure the convergence of the mediumband channel to a narrowband channel as $T_m \to 0$.

$$\eta_o = \sqrt{\left(1-\frac{\beta}{4}\right)\left[\left(\sum_{n=0}^{N-1}|\gamma_n|^2\right) - |h_o|^2\right] + \sum_{n=0}^{N-1}\sum_{\substack{m=0 \\ m\neq n}}^{N-1}\gamma_n\gamma_m^* R(\tau_n-\tau_m)}. \tag{16}$$

$$R(\tau) = \operatorname{sinc}\left(\frac{\tau}{T_s}\right)\frac{\cos\left(\beta\frac{\pi\tau}{T_s}\right)}{1-\left(\frac{2\beta\tau}{T_s}\right)^2} - \frac{\beta}{4}\operatorname{sinc}\left(\beta\frac{\tau}{T_s}\right)\frac{\cos\left(\frac{\pi\tau}{T_s}\right)}{1-\left(\frac{\beta\tau}{T_s}\right)^2}. \tag{17}$$

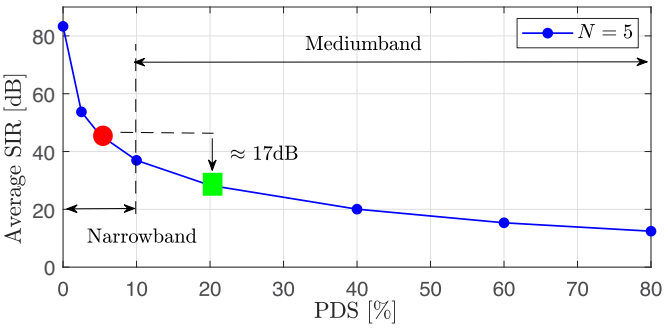

FIGURE 5. SIR vs percentage delay spread of mediumband wireless channels, where $\beta = 0.8$ and $N = 5$. Here T_m is varied appropriately to achieve different PDSs while keeping $T_s = 1$.

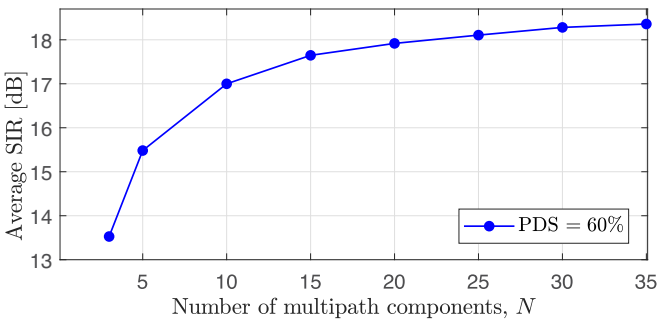

FIGURE 6. SIR vs N of mediumband channels, where $\beta = 0.8$ and the percentage delay spread is 60%. Here $T_s = 1$ and $T_m = 0.6$.

B. CROSS-CORRELATION OF DESIRED SIGNAL AND INTERFERENCE

Let's consider the cross-correlation of the desired signal, $h_o s(t-\hat{\tau})$ and the interference signal, $\eta_o u(t)$: $\mathcal{E}\{\overline{h_o s(t-\hat{\tau})}\eta_o u(t)\}$, where the "overline" denotes the complex conjugation. This cross-correlation can equivalently be expressed by:

$$\begin{aligned}\mathcal{L} &= \mathcal{E}\left\{\overline{h_o s\big(t-\hat{\tau}\big)}\eta_o u(t)\right\},\\ &= \mathcal{E}\left\{\overline{\sqrt{E_s}h_o s\big(t-\hat{\tau}\big)}\Big(r(t)-\sqrt{E_s}h_o s\big(t-\hat{\tau}\big)\Big)\right\}. \quad (20)\end{aligned}$$

The expectation operation with respect to the random process, $s(t)$, yields:

$$\mathcal{L} = E_s\left[h_o^*\left(\sum_{n=0}^{N-1}\gamma_n R\big(\tau_n-\hat{\tau}\big)\right) - |h_o|^2\left(1-\frac{\beta}{4}\right)\right]. \quad (21)$$

From (15), it is known that $\sum_{n=0}^{N-1}\gamma_n R(\tau_n-\bar{\tau}) = h_o(1-\frac{\beta}{4})$, which in turn confirms that if h_o is chosen optimally as given in (15), the correlation between the desired signal and the interference signal would be zero.

IV. SIGNAL-TO-INTERFERENCE-RATIO (SIR)

The quality of mediumband channels can be quantified using a metric like the average signal-to-interference-ratio (SIR), which can be evaluated using:

$$\text{Average SIR} = \frac{\mathcal{E}\left\{\left|h_o s\big(t-\hat{\tau}\big)\right|^2\right\}}{\mathcal{E}\left\{|\eta_o u(t)|^2\right\}}, \quad (22)$$

where the expectations in both the numerator and the denominator are over both $s(t)$ and all the propagation parameters. Due to the independence of the fading process and the channel input process $s(t)$, the expectations in (22) can be evaluated in two steps. The expectation over the input process is firstly evaluated while keeping the propagation parameters $\Gamma = \{\alpha_n, \phi_n, \tau_n\}$ fixed. The quantity $\hat{\tau}$ is chosen optimally using exhaustive search, h_o is from (15), and η_o is from (16). Secondly, the expectation over the fading process is evaluated by repeating the first step until sufficiently stable values are obtained.

Fig. 5 shows the average SIR performance of a mediumband wireless channel for different PDSs. As also described in Section II-A, different PDSs are achieved by changing T_m appropriately according to (4) while keeping $T_s = 1$. It can be seen clearly that the SIR gradually decreases as the PDS increases. Furthermore, as shown in Fig. 6, as N increases, the average SIR increases, but quickly saturates (see $N > 20$ in Fig. 6). Many more insights can also be drawn from these performance results.

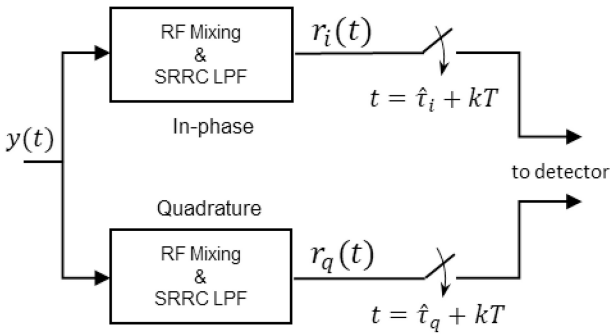

FIGURE 7. A schematic diagram of a digital wireless receiver with separate I/Q processing, where T is the sampling period.

As shown in Fig. 5, when the PDS is less than 10%, the narrowband condition is deemed to be satisfied. The larger region where the PDS is greater than 10% is the mediumband region. It is clearly many times as wide as the narrowband region. For a given spatially averaged delay profile, one can design either a narrowband or a mediumband system by choosing an appropriate symbol period. The RED circle (i.e., PDS = 5%) in Fig. 5 represents a narrowband system, while the GREEN square (i.e., PDS = 20%) represents a mediumband system. The signaling rate of the mediumband system at the GREEN square is 4 times as high as the signalling rate of the narrowband system at the RED circle. If all other aspects such as the modulation schemes of two systems are the same, this means a potential data rate 4 times as high as the data rate of the narrowband system operating at the RED circle. On the flipside however, the mediumband system at the GREEN square is exposed to about 17dB more interference, which is typically undesirable. However, in the coming sections, we see that mediumband channels have the potential to mitigate this excessive interference successfully by themselves.

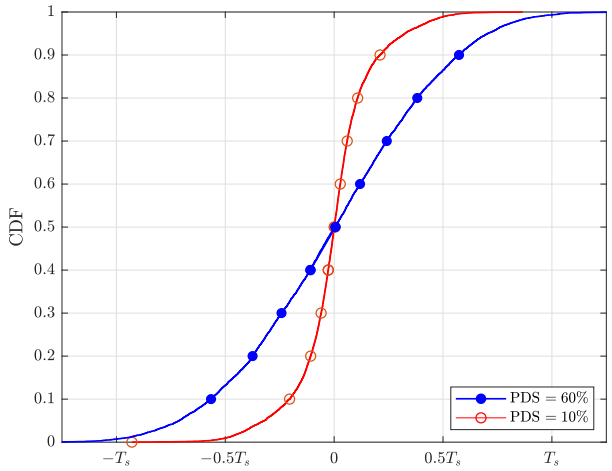

FIGURE 8. CDF of $\hat{\tau}_i - \hat{\tau}_q$ of mediumband wireless channels for PDS = 10% and 60%, where $\beta = 0.8$ and $N = 5$.

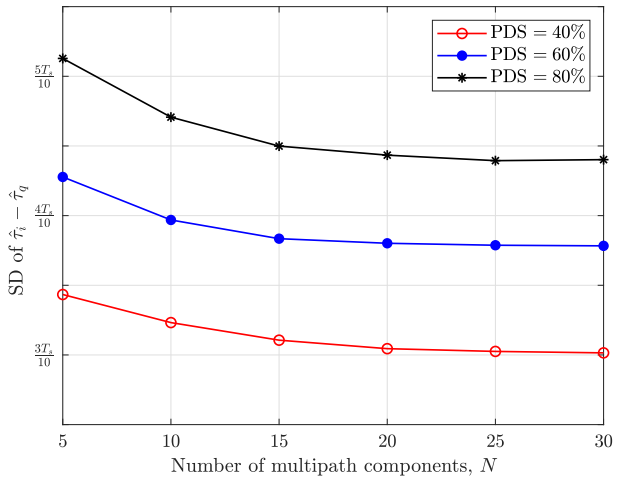

FIGURE 10. Variation of the SD of $\hat{\tau}_i - \hat{\tau}_q$ for different Ns, where $\beta = 0.8$, and three different PDSs (i.e., 40%, 60%, 80%) are considered.

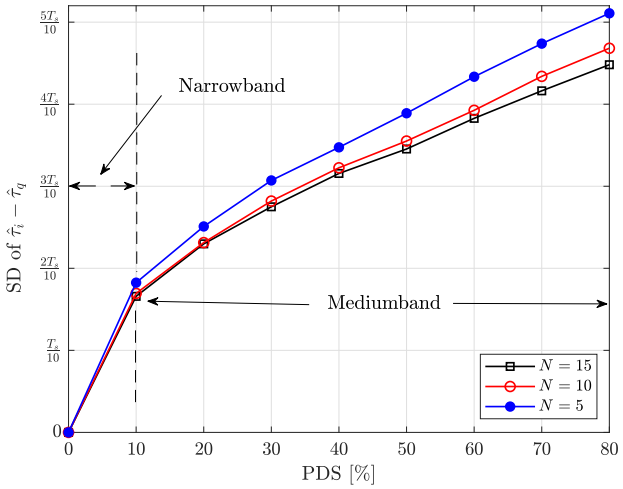

FIGURE 9. SD of $\hat{\tau}_i - \hat{\tau}_q$ against the percentage delay spread of mediumband wireless channels for different N, where $\beta = 0.8$.

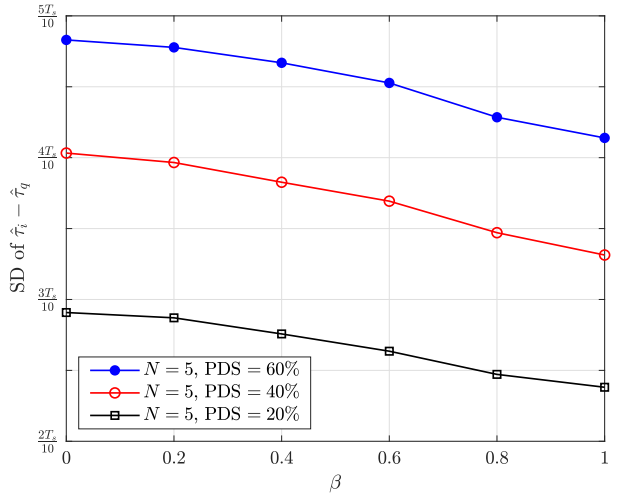

FIGURE 11. Variation of the SD of $\hat{\tau}_i - \hat{\tau}_q$ for different βs, where $N = 5$, and three different PDSs (i.e., 20%, 40%, 60%) are considered.

V. I/Q PROCESSING

In digital wireless communication, I/Q processing typically includes RF mixing, receive filtering (i.e., SRRC low-pass filtering), synchronization, and I/Q sampling [36]. Some simpler systems might use the same time synchronization and sampling for both the in-phase (i.e., "I") and the quadrature-phase (i.e., "Q") branches, but as shown in Fig. 7, the RF mixing and the receiver filtering can also be applied to the I and Q branches separately. In this paper, such separate time synchronization and I/Q sampling are assumed.

In I/Q sampling, the I and Q branches of the RX firstly synchronize to I/Q signals $r_i(t)$ and $r_q(t)$ separately. These I/Q signals are subsequently sampled in regular intervals. Let the sampling instances of the I and Q branches respectively be $\hat{\tau}_i + lT$ and $\hat{\tau}_q + lT$, where T is the sampling period at the RX, and $\hat{\tau}_i$ and $\hat{\tau}_q$ are respectively the time instances, which the I and Q branches of the RX synchronize to. Consider the baseband equivalent I/Q signals:

$$r_i(t) = \sqrt{E_s} \sum_{n=0}^{N-1} \alpha_n \cos(\phi_n) s(t - \tau_n), \tag{23}$$

$$r_q(t) = -\sqrt{E_s} \sum_{n=0}^{N-1} \alpha_n \sin(\phi_n) s(t - \tau_n), \tag{24}$$

where it is assumed that $s(t)$ is a real signal, which is indeed the case in single dimensional modulations like BPSK, 4-PAM, etc. It is clear that $r_i(t)$ and $r_q(t)$ are nothing but differently weighted sum of the same set of signals, which indicates that $\hat{\tau}_i$ and $\hat{\tau}_q$ should be different.

As shown in Figs. 8-11, in the narrowband regime, the difference, $\hat{\tau}_i - \hat{\tau}_q$ is negligible, but in the mediumband regime, as the degree of mediumband-ness increases, the significance of this difference increases rapidly. Hence, mediumband wireless systems require separate I/Q synchronizations.

In Theorem 1, $\hat{\tau}_i = \hat{\tau}_q = \hat{\tau}$ is assumed. If I/Q branches at the RX are assumed to be synchronized to $\hat{\tau}_i$ and $\hat{\tau}_q$ respectively, Theorem 1 can be elaborated in the absence of

AWGN to highlight the effect of different $\hat{\tau}_i$ and $\hat{\tau}_q$ as:

$$\begin{bmatrix} r_i(t) \\ r_q(t) \end{bmatrix} = \sqrt{E_s}\begin{bmatrix} h_o^i s(t-\hat{\tau}_i) \\ h_o^q s(t-\hat{\tau}_q) \end{bmatrix} + \sqrt{E_s}\begin{bmatrix} \eta_o^i u_i(t) \\ \eta_o^q u_q(t) \end{bmatrix}, \quad (25)$$

where $r(t) = r_i(t) + jr_q(t)$ is the baseband equivalent received signal; $u(t) = u_i(t) + ju_q(t)$ is uncorrelated zero mean unit variance (per dimension) interference signal; and $h_o = h_o^i + jh_o^q$ is given by:

$$\mathrm{Re}\{h_o\} = h_o^i = \frac{\sum_{n=0}^{N-1} \mathrm{Re}\{\gamma_n\} R(\tau_n - \hat{\tau}_i)}{1 - 0.25\beta}, \quad (26a)$$

$$\mathrm{Im}\{h_o\} = h_o^q = \frac{\sum_{n=0}^{N-1} \mathrm{Im}\{\gamma_n\} R(\tau_n - \hat{\tau}_q)}{1 - 0.25\beta}; \quad (26b)$$

where η_o^i & η_o^q are given in (27), as shown at the bottom of the page.

By following the same procedure described in the Appendix on the following mean-squared-error for the I and Q branches separately:

$$J_i = \mathcal{E}\left\{ \left| r_i(t) - \sqrt{E_s} h^i s(t-\hat{\tau}_i) \right|^2 \middle| \Gamma, h^i \right\}, \quad (28a)$$

$$J_q = \mathcal{E}\left\{ \left| r_q(t) - \sqrt{E_s} h^q s(t-\hat{\tau}_q) \right|^2 \middle| \Gamma, h^q \right\}, \quad (28b)$$

one can arrive at the channel model in (25), where the optimum values for h^i and h^q are available in (26). Also, on the one hand, as $T_m \to 0$, $|\hat{\tau}_i - \hat{\tau}_q| \to 0$, and on the other hand, the mediumband channel model in (25) also reduces to the narrowband model, which is (12).

Fig. 8 shows the cumulative distribution functions (CDFs) of $\hat{\tau}_i - \hat{\tau}_q$ for two representative percentage delay spreads, where the quantities $\hat{\tau}_i$ and $\hat{\tau}_q$ are chosen optimally using exhaustive search applied to the I and Q branches separately. One can clearly see in Fig. 8 that, the larger the delay spread, the greater the dispersion of $\hat{\tau}_i - \hat{\tau}_q$. It is also clear that when PDS = 10%, $\hat{\tau}_i - \hat{\tau}_q$ is often close to zero, and it is very unlikely to go above $0.5T_s$. However, when PDS = 60%, $\hat{\tau}_i - \hat{\tau}_q$ is very likely to go above $0.5T_s$. In fact from Fig. 8, $\Pr(|\hat{\tau}_i - \hat{\tau}_q| \geq 0.5T_s) = 0.27$.

Fig. 9 captures the degree of dispersion of $\hat{\tau}_i - \hat{\tau}_q$ in mediumband channels through the standard deviation (SD) of $\hat{\tau}_i - \hat{\tau}_q$, where the SD is shown against the PDS. When PDS $\leq$ 10%, the difference between $\hat{\tau}_i$ and $\hat{\tau}_q$ is not significant, but as the PDS increases beyond the narrowband region, the SD of the difference $\hat{\tau}_i - \hat{\tau}_q$ increases steadily. It can also be seen that the rate of increase of the SD of $\hat{\tau}_i - \hat{\tau}_q$ is greater for lower N.

Fig. 10 exhibits the effect of the number of dominant multipath components (i.e., N) on the variation of the SD of $\hat{\tau}_i - \hat{\tau}_q$, and Fig. 11 shows the effect of pulse shaping (i.e., β) on the variation of SD of $\hat{\tau}_i - \hat{\tau}_q$, where different PDS scenarios are considered in both simulations. It can be seen in Fig. 10 that, the effect of the number of multipath components on the SD of $\hat{\tau}_i - \hat{\tau}_q$ reduces as N increases. However, the effect of N on $\hat{\tau}_i - \hat{\tau}_q$ is not as significant as the effect of PDS on $\hat{\tau}_i - \hat{\tau}_q$. Similarly, from Fig. 11, it can be seen that the effect of β on the SD of $\hat{\tau}_i - \hat{\tau}_q$ also reduces as β increases. However, the effect of β and N on $\hat{\tau}_i - \hat{\tau}_q$ is not as significant as the effect of PDS on $\hat{\tau}_i - \hat{\tau}_q$.

VI. BIT ERROR RATE PERFORMANCE

The information transmission as reliably as possible is the main function of any communication system. It is the average bit error rate, which is typically used to quantify the level of reliability [26]. Using the model in Theorem 1, in this section, mediumband channels are studied and compared with classical narrowband channels in terms of BER. Unlike the narrowband channels, which is ISI free, as shown in (13), mediumband channels appear to have an inherent handicap, which is the additive ISI. This ISI increases as the degree of mediumband-ness (or PDS) increases, which is even worse. However, the results herein indicate that the story is not as bleak as Fig. 5 shows due to an inherent characteristic of mediumband channels, which appears to counteract this ISI successfully.

In order to evaluate BER performance, discrete-time versions of the corresponding channel models are used, where we start with the narrowband case. Extending the channel model in (12), the received baseband equivalent signal with AWGN becomes [27]:

$$r'(t) \approx \sqrt{E_s} g_o s(t-\hat{\tau}) + n(t), \quad (29)$$

where $n(t)$ is the complex zero mean AWGN signal, where $\mathcal{E}\{|n(t)|^2\} = \sigma^2$. Assuming that the RX synchronizes to the common delay $\hat{\tau}$ perfectly, and appropriately samples $r'(t)$ afterward, a discrete-time version of $r'(t)$, $r'(k)$ is obtained [16]. Using these samples, one can detect the kth information symbol using the statistic [17, eq. (3.17)]:

$$\Delta_{NB}(k) = \mathrm{Re}\left(\frac{g_o^H r'(k)}{\sqrt{E_s}|g_o|^2} \right), \quad (30)$$

$$\eta_o^i = \sqrt{\left(1 - \frac{\beta}{4}\right)\left[\left(\sum_{n=0}^{N-1} \mathrm{Re}\{\gamma_n\}^2\right) - \left(h_o^i\right)^2\right] + \sum_{n=0}^{N-1}\sum_{\substack{m=0 \\ m\neq n}}^{N-1} \mathrm{Re}\{\gamma_n\}\mathrm{Re}\{\gamma_m\} R(\tau_n - \tau_m)}. \quad (27a)$$

$$\eta_o^q = \sqrt{\left(1 - \frac{\beta}{4}\right)\left[\left(\sum_{n=0}^{N-1} \mathrm{Im}\{\gamma_n\}^2\right) - \left(h_o^q\right)^2\right] + \sum_{n=0}^{N-1}\sum_{\substack{m=0 \\ m\neq n}}^{N-1} \mathrm{Im}\{\gamma_n\}\mathrm{Im}\{\gamma_m\} R(\tau_n - \tau_m)}. \quad (27b)$$

where the operator $(.)^H$ denotes the complex conjugate operation. In order to do this information detection reliably, typically the wireless RX should have some knowledge about the fading factor g_o. In modern wireless communication, this factor can be estimated very accurately, and the knowledge of the propagation parameters of the individual multipath components (i.e., α_ns, ϕ_ns and τ_ns) is not required [14], [15]. In this paper, we assume that g_o is perfectly known at the RX [17].

A. DISCRETE-TIME MEDIUMBAND CHANNEL

The channel model described in Theorem 1 is a continuous-time version, and the corresponding discrete-time version can be derived by sampling $r'(t)$ in (14) appropriately. If it is assumed that, the RX is synchronized separately as described in Section V and $r'(t)$ is sampled at regular intervals afterwards the discrete-time mediumband channel becomes:

$$\begin{bmatrix} r'_i(k) \\ r'_q(k) \end{bmatrix} = \sqrt{E_s}\begin{bmatrix} h^i_o s(k) \\ h^q_o s(k) \end{bmatrix} + \begin{bmatrix} \sqrt{E_s}\eta^i_o u_i(k) + n_i(k) \\ \sqrt{E_s}\eta^q_o u_q(k) + n_q(k) \end{bmatrix}, \quad (31)$$

where it is assumed that the I and Q branches are sampled at $t = \hat{\tau}_i + kT$ and $t = \hat{\tau}_q + kT$ respectively. The vector equation in (31) can be simplified to:

$$r'(k) = \sqrt{E_s} h_o s(k) + \tilde{n}(k), \quad (32)$$

where $r'(k) = r'_i(k) + jr'_q(k)$ and $s(k)$ are the kth samples of $r'(t)$ and $s(t)$ respectively. The $\tilde{n}(k)$ is the residual ISI plus AWGN sample obtained from the second term of the right-hand-side (RHS) of (31). Furthermore, h_o in the presence of separate I/Q processing is available in (26).

B. BER EVALUATION

Similar to the case in narrowband channels, assuming the RX has the perfect knowledge of h_o, the sufficient statistic to detect the kth BPSK symbol is:

$$\Delta_{MB}(k) = \mathrm{Re}\left(\frac{h^H_o r'(k)}{\sqrt{E_s}|h_o|^2} \right), \quad (33)$$

and the kth detected symbol hence is:

$$\hat{I}_k = \begin{cases} 1, & \Delta_{NB}(k) > 0, \\ -1, & \Delta_{NB}(k) < 0. \end{cases} \quad (34)$$

The decision statistic in (30) for narrowband channels is optimum in maximum likelihood (ML) sense [17, Sec. 3.1], but the decision statistic and the corresponding rule in (33) and (34) respectively for mediumband channels may not be optimum. However, in order to have a fairer comparison of channels, the rule in (34) is used henceforth.

Fig. 12 shows the average BER of BPSK modulation in mediumband channels, where mediumband channels with different degrees of mediumband-nesses are considered. The number of multipath components and the roll-off factor are set to $N = 10$ and $\beta = 0.22$ respectively, which is typically the technical specification of ETSI and 3GPP for radio transmission and reception [35]. As described in (4), the degree of mediumband-ness is given in terms of PDS, and the receive SNR is defined by:

$$\mathrm{SNR} = \frac{\mathcal{E}\{|r(t)|^2\}}{\mathcal{E}\{|n(t)|^2\}} = \frac{\mathcal{E}\{|r(t)|^2\}}{\sigma^2}. \quad (35)$$

The expectation in the numerator of (35) is over both $s(t)$ and all the propagation parameters.

For comparison, the average BER of BPSK modulation in a narrowband channel is also included (RED curve). This narrowband channel is obtained by setting $T_m = 0$ and thus PDS $= 0\%$, which basically means the excess delay of all the multipath components are the same, that is $\tau_0 = \tau_1 = \cdots = \tau_{N-1}$. This ensures the perfect zero ISI scenario described in (12) and (29). In this case, as N increases, g_o is normally distributed, corresponding to Rayleigh fading. The average BER in BPSK can thus be analytically given by [27], [40]:

$$\text{Average BER} = 0.5\left(1 - \sqrt{\frac{\mathrm{SNR}}{1+\mathrm{SNR}}}\right). \quad (36)$$

It is this fundamental limit, which the average BER of mediumband channels considered in this paper are compared against.

Despite having increased level of ISI, it is clear from Fig. 12 that, surprisingly, the average BER performance of mediumband channels is significantly better than that of the classical narrowband channel. For instance, the mediumband channel of PDS $= 20\%$ outperforms the narrowband channel up to an SNR as high as 35dB, and the average BER gain in some SNRs can be as high as 4dB. As expected, the effect of ISI is clearly visible, but its effect appears to kick-in notably at very high SNR values (after 30dB in PDS $= 20\%$ case), which are typically outside the usual operating region of the most wireless communication systems. Furthermore, the mediumband channel of PDS $= 60\%$, which has significantly high level of ISI (see Fig. 5), even outperforms the narrowband channel in terms of average BER up to an SNR of 25dB (see the BLACK curve).

Also, it can be seen in Fig. 12 that the mediumband channel of PDS $= 60\%$ outperforms the mediumband channel of PDS $= 20\%$ up to an SNR of 20dB, where the gain achieved in some SNRs can be over 1dB. Fig. 13 shows the average BER performance for the same scenarios considered in Fig. 12, but for $\beta = 0.5$. We can see that the BER trends are the same, but the gain margin is reduced. However, the mediumband channel of PDS$=$ 60% now outperforms the ideal narrowband channel even up to an SNR of 30dB, which is an increase of 5dB over the same channel with $\beta = 0.22$. What actually causes this?

C. EFFECT OF DEEP FADING AVOIDANCE

In [17, p. 70], Tse and Viswanath point out that, "$\cdots$ *the main reason why detection in fading channel has poor performance is not because of the lack of knowledge of the channel at the receiver. It is due to the fact that the channel gain is random and there is a significant probability that the*

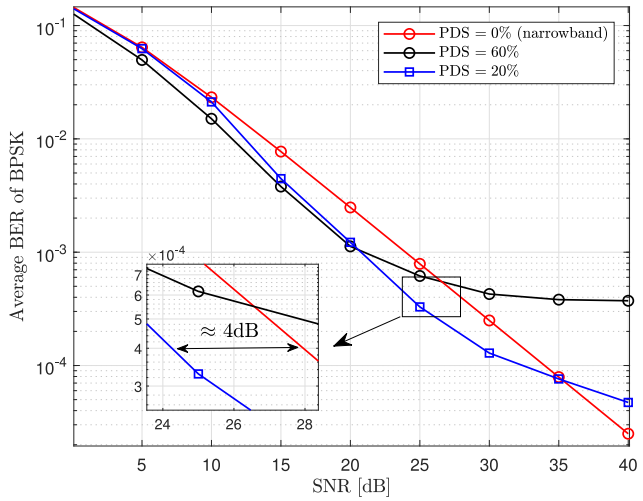

FIGURE 12. Average BER of BPSK modulation in mediumband channels for different percentage delay spreads, where $\beta = 0.22$ and $N = 10$. Here PDS= 0% represents an ideal narrowband channel with no ISI.

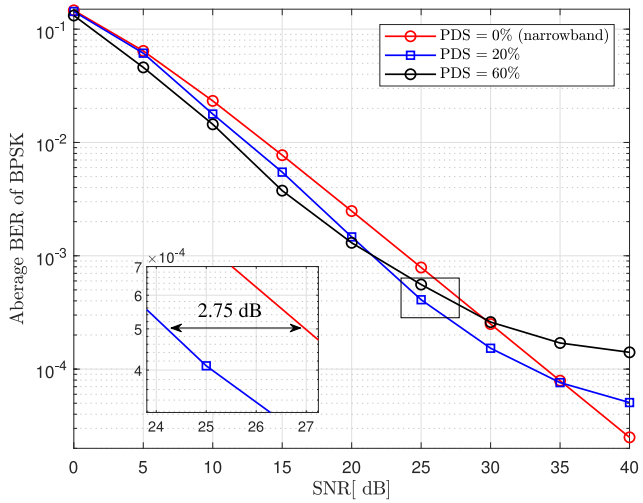

FIGURE 13. Average BER of BPSK modulation in mediumband wireless channels for different percentage delay spreads, where $\beta = 0.5$ and $N = 10$.

channel is in a deep fade", and this effect of deep fading is a major, well-documented challenge in wireless communication [17], [37], [38], [39]. In this section, we see that as far as the deep fading is concerned, operating in the mediumband regime may be extremely beneficial.

In Figs. 14-16, the statistical properties of the fading factors of the desired signal of both the narrowband (i.e., g_o) and the mediumband channel (i.e., h_o) are compared. In Fig. 14, cumulative distribution functions (CDFs) of the squared magnitudes are considered, but they appear to not explain the BER trends observed in Figs. 12 and 13. We also consider the CDFs of $\mathrm{Re}(h_o)$ and $\mathrm{Re}(g_o)$ in Fig. 15.[4] In this case, the CDFs of $\mathrm{Re}(h_o)$ clearly exhibits some unusual trends. This particular behaviour is more prominent in Fig. 16, where the probability density functions (PDFs)

4. Both g_o and h_o are complex quantities, and the real part is chosen arbitrarily. Similar statistical trends are observed for the imaginary part too.

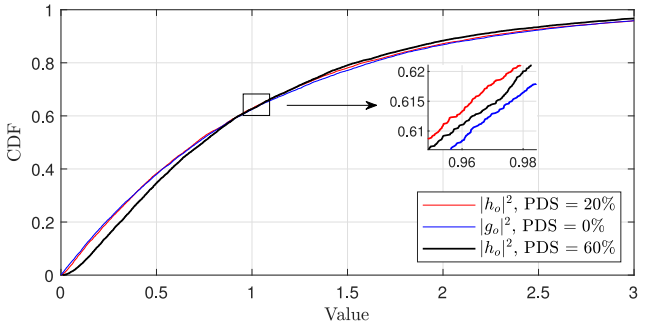

FIGURE 14. CDF of the squared magnitude of desired fading factors of mediumband and narrowband channels, where $\beta = 0.22$ and $N = 10$.

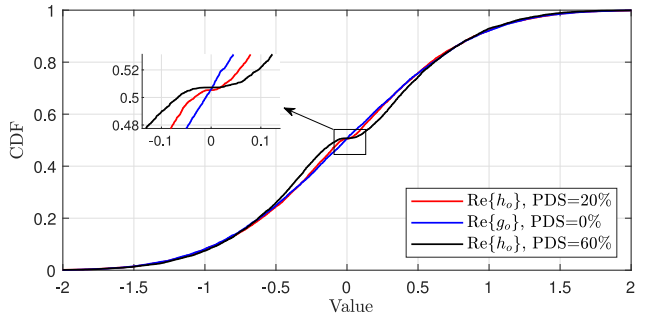

FIGURE 15. CDF of the real dimension of desired fading factors of mediumband and narrowband channels, where $\beta = 0.22$ and $N = 10$.

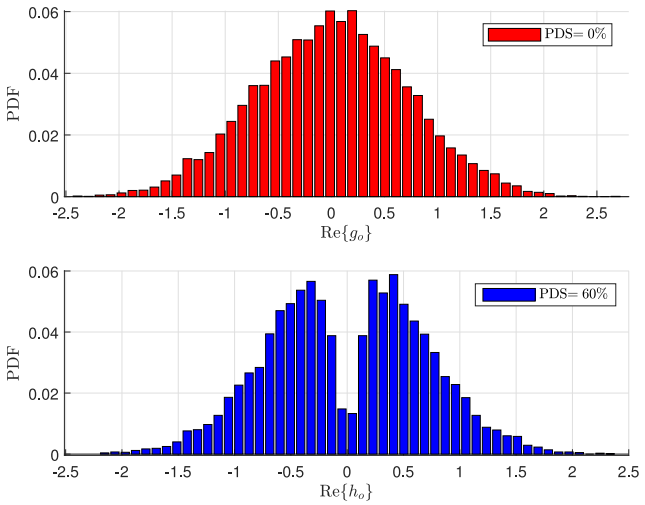

FIGURE 16. PDF of the real dimension of desired fading factors of a mediumband channel and the narrowband channel, where $\beta = 0.22$ and $N = 10$.

of $\mathrm{Re}(h_o)$ and $\mathrm{Re}(g_o)$ are shown. In this case, the probability of deep fading in the mediumband channel appears to be lower than that of the ideal narrowband channel (due to the trench in the middle). If one, who skims over the fading factors:

$$\mathrm{Re}\{h_o\} = \frac{\sum_{n=0}^{N-1} \alpha_n \cos\phi_n R\left(\tau_n - \hat{\tau}_i\right)}{1 - 0.25\beta}, \tag{37}$$

$$\mathrm{Re}\{g_o\} = \sum_{n=0}^{N-1} \alpha_n \cos\phi_n, \tag{38}$$

TABLE 1. The quantification of the deep fading avoidance effect in mediumband channels.

PDS [%]	$\Pr(\lvert\mathrm{Re}\{h_o\}\rvert \le 0.2)$		
	$\beta = 0.8$	$\beta = 0.5$	$\beta = 0.22$
20	0.2038	0.2030	0.1987
40	0.1617	0.1612	0.1519
60	0.1316	0.1273	0.1204

may notice that $\mathrm{Re}\{h_o\}$ is a weighted sum, whereas $\mathrm{Re}\{g_o\}$ is a regular sum. On closer inspection, one may find that the weights $R(\tau_n - \hat{\tau}_i)$ are in fact not just scalers, but random variables that are highly dependent on the underlying propagation parameters in very complicated ways. It is this complex, yet interesting, relation of $\mathrm{Re}\{h_o\}$ with the underlying multipath components that statistically reduces the deep fading in mediumband channels giving notable average BER performance gains exhibited in Figs. 12 and 13.

Table 1 furthermore quantifies the extent of the effect of deep fading avoidance of mediumband channels. It is based on measurements of the probability of the magnitude of $\mathrm{Re}\{h_o\}$ falling below a certain threshold using a Monte-Carlo simulation with 50000 iterations. For the narrowband channel, the path gain normalization (i.e., $\alpha_n \propto 1/\sqrt{N}$) ensures that: $\mathrm{Mean}(\mathrm{Re}\{g_o\}) = 0$, $\mathrm{Var}(\mathrm{Re}\{g_o\}) = 0.5$, and:

$$\Pr(|\mathrm{Re}\{g_o\}| \le 0.2) = 0.2214, \tag{39}$$

which in fact corresponds to the classical Rayleigh fading scenario [40]. As shown in Table 1, the quantity $\Pr(|\mathrm{Re}\{h_o\}| \le 0.2)$ decreases as the PDS increases, which quantitatively confirms the effect of deep fading avoidance in mediumband channels.

The BER performance of mediumband systems is a result of a complex interplay between the ISI and the effect of deep fading avoidance. In low SNR, the effect of deep fading avoidance is dominant and overpowers ISI, but as the SNR increases, as expected the effect of ISI eventually kicks-in.

VII. GENERALIZED MEDIUMBAND CHANNELS

The discussion so far was about the most basic scenario where mediumband channels can occur, but mediumband channels can also occur in many other scenarios. As depicted in Fig. 17, consider a propagation environment such that $T_m \approx 1.2T_s$, that is PDS $\approx 120\%$. Typically, this multipath scenario is modelled (because $1 < T_m/T_s < 2$) by using a broadband channel model with two fading factors (i.e., taps)

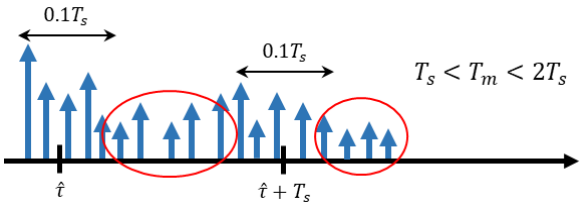

FIGURE 17. A 2-tap broadband channel with elements of mediumband-nesses that gives rise to a channel that may be called a generalized mediumband channel. The $\hat{\tau}$ is assumed to be the time that the RX is synchronized to, and the taps are exactly T_s apart. It is the multipath components circled in RED that significantly contribute to the model mismatch error $\sqrt{E_s}\zeta_o u(t)$ in (46).

as [28][5]:

$$r(t) \approx \sqrt{E_s}h_1 s\big(t - \hat{\tau}\big) + \sqrt{E_s}h_2 s\big(t - \hat{\tau} - T_s\big), \tag{40}$$

where the two taps h_1 and h_2 are exactly separated by T_s. Note that for notational simplicity, we assume that $\hat{\tau} = \hat{\tau}_i = \hat{\tau}_q$, but this difference will be brought to fore subsequently in (55). The multipath components that are closer, typically within $\pm 0.05T_s$ to these taps, are successfully captured by this model. The multipath components that are located further away (e.g., within red circles) are left poorly accounted by these taps.

Following a similar approach in the Appendix, the optimum tap weights in minimum-mean-squared-error sense can be found. We consider the following mean-squared-error:

$$J = \mathcal{E}\big\{|e(t)|^2 \big| \Gamma, h_1, h_2\big\}, \tag{41}$$

where $e(t) = r(t) - \sum_{v=1}^{2}\sqrt{E_s}h_v s(t - \hat{\tau} - (v-1)T_s)$. In light of (61), J in (41) can be simplified to get (42), as shown at the bottom of the page. Taking the derivatives with respect to h_1 and h_2 separately, J in (42) can be further optimized resulting:

$$\psi_0 h_1^i + \psi_1 h_2^i = \sum_{n=0}^{N-1}\mathrm{Re}\{\gamma_n\}R\big(\tau_n - \hat{\tau}\big), \tag{43a}$$

$$\psi_1 h_1^i + \psi_0 h_2^i = \sum_{n=0}^{N-1}\mathrm{Re}\{\gamma_n\}R\big(\tau_n - \hat{\tau} - T_s\big), \tag{43b}$$

5. This model is preferred, because it is this model which, after synchronization and sampling, leads to the well-known convolution sum formula, and forms the basis of Fast Fourier Transform (FFT) based multi-carrier modulation schemes like SC-FDM and OFDM for broadband channels [27, Sec. 12.4].

$$J = E_s\Bigg[\bigg(1 - \frac{\beta}{4}\bigg)\bigg(\sum_{v=1}^{2}|h_v|^2 + \sum_{n=0}^{N-1}|\gamma_n|^2\bigg) + \sum_{n=0}^{N-1}\sum_{\substack{m=0\\ m\neq n}}^{N-1}\gamma_n\gamma_m^* R(\tau_n - \tau_m) + 2\psi_1\mathrm{Re}\big\{h_1 h_2^*\big\} - \sum_{v=1}^{2}\sum_{n=0}^{N-1}2\mathrm{Re}\big\{\gamma_n^* h_v\big\}R\big(\tau_n - \hat{\tau} - (v-1)T_s\big)\Bigg]. \tag{42}$$

where for notational simplicity $\psi_l = R(lT_s)$ for $l = 0, 1, \ldots,$ and

$$\psi_0 h_1^q + \psi_1 h_2^q = \sum_{n=0}^{N-1} \mathrm{Im}\{\gamma_n\} R\big(\tau_n - \hat{\tau}\big), \tag{44a}$$

$$\psi_1 h_1^q + \psi_0 h_2^q = 7 \sum_{n=0}^{N-1} \mathrm{Im}\{\gamma_n\} R\big(\tau_n - \hat{\tau} - T_s\big). \tag{44b}$$

Here the superscripts, "i" and "q" in (43) and (44) denote the real and imaginary parts of the corresponding complex numbers. Solving these sets of simultaneous equations, the optimum tap weights $(h_1)_o$ and $(h_2)_o$ can be obtained as shown in (45), as shown at the bottom of the page, where $(.)_o$ denotes the optimal value of the argument.

As a result, a more suitable and accurate channel model for the broadband channel depicted in Fig. 17 may in the absence of the noise be given by:

$$r(t) = \sqrt{E_s}(h_1)_o s\big(t - \hat{\tau}\big) + \sqrt{E_s}(h_2)_o s\big(t - \hat{\tau} - T_s\big) + \sqrt{E_s}\zeta_o u(t), \tag{46}$$

where ζ_o is given in (47), as shown at the bottom of the page, and $u(t)$ is a zero mean, unit variance interference signal or more accurately the model mismatch error signal. This $u(t)$ inherits the statistical properties of $s(t)$.

Since the channel model in (46) has all the hallmarks of the mediumband model in Theorem 1, but with multiple taps, this model may be categorized as a "***generalized mediumband channel***" that falls between the broadband channels of 2 and 3 taps. If the conventional narrowband channel is assumed to be nothing but a broadband channel with a single tap, the original mediumband channel described in Theorem 1 is a generalized mediumband channel between the broadband channels of one and two taps. Hence in other words, this paper studies the broadband channels when transitioning from L taps to $L+1$ taps, where $L = 1, 2, 3, \ldots$

The cross-correlation of the desired signal that is $\sum_{v=1}^{2}(h_v)_o s(t - \hat{\tau} - (v-1)T_s)$ and the interference signal that is $\zeta_o u(t)$ can be expressed by:

$$\mathcal{L} = \mathcal{E}\left\{\left(\sum_{v=1}^{2}(h_v)_o s\big(t - \hat{\tau} - (v-1)T_s\big)\right)\overline{\zeta_o u(t)}\right\}, \tag{50}$$

where $\sqrt{E_s}$ factors shown alongside the desired and the interference signals in (46) are dropped for brevity. The expectation with respect to the random process $s(t)$ yields:

$$\mathcal{L} = \left[\sum_{v=1}^{2}\sum_{n=0}^{N-1}(h_v)_o \gamma_n^* R\big(\tau_n - \hat{\tau} - (v-1)T_s\big) - \sum_{v=1}^{2}\sum_{l=1}^{2}(h_v)_o (h_l)_o^* R((v-l)T_s)\right]. \tag{51}$$

We can see that if and only if $(h_v)_o$ for $v = 1, 2$ are chosen optimally according to (45), the correlation between the desired signal and the interference signal would be zero.

Fig. 18 shows the extent of the deep fading avoidance effect in different taps of the generalized mediumband channel, where the PDFs of $\mathrm{Re}\{(h_1)_o\}$ and $\mathrm{Re}\{(h_2)_o\}$ in (46) are shown. The effect of deep fading avoidance is prominent, but appears to occur in one of the taps only, which in this case is the first tap. The simulations further show that the occurrence of the deep fading avoidance can be shifted from the first tap to the second tap if needed. However, further research is needed to understand how the effect of deep fading avoidance in generalized mediumband channels can be finely manipulated and fully harnessed for future wireless communication.

The analysis here can be extended to the general case of $L = \lceil T_m/T_s \rceil$ taps and the result is summarised in the following Corollary.

Corollary 1: If a generalized mediumband channel is such that $\lceil T_m/T_s \rceil = L$, the baseband equivalent received signal

$$(h_1)_o = \frac{\psi_0\left(\sum_{n=0}^{N-1}\gamma_n R\big(\tau_n - \hat{\tau}\big)\right) - \psi_1\left(\sum_{n=0}^{N-1}\gamma_n R\big(\tau_n - \hat{\tau} - T_s\big)\right)}{\psi_0^2 - \psi_1^2} \tag{45a}$$

$$(h_2)_o = \frac{-\psi_1\left(\sum_{n=0}^{N-1}\gamma_n R\big(\tau_n - \hat{\tau}\big)\right) + \psi_0\left(\sum_{n=0}^{N-1}\gamma_n R\big(\tau_n - \hat{\tau} - T_s\big)\right)}{\psi_0^2 - \psi_1^2} \tag{45b}$$

$$\zeta_o = \left[\psi_0\left(\sum_{v=1}^{2}|(h_v)_o|^2 + \sum_{n=0}^{N-1}|\gamma_n|^2\right) + \sum_{n=0}^{N-1}\sum_{\substack{m=0\\ m\neq n}}^{N-1}\gamma_n\gamma_m^* R(\tau_n - \tau_m) + \sum_{v=1}^{2}\sum_{\substack{l=1\\ l\neq i}}^{2}(h_v)_o (h_l)_o^* R((v-l)T_s) - \sum_{v=1}^{2}\sum_{n=0}^{N-1} 2\mathrm{Re}\big\{\gamma_n^*(h_v)_o\big\} R\big(\tau_n - \hat{\tau} - (v-1)T_s\big)\right]^{\frac{1}{2}}. \tag{47}$$

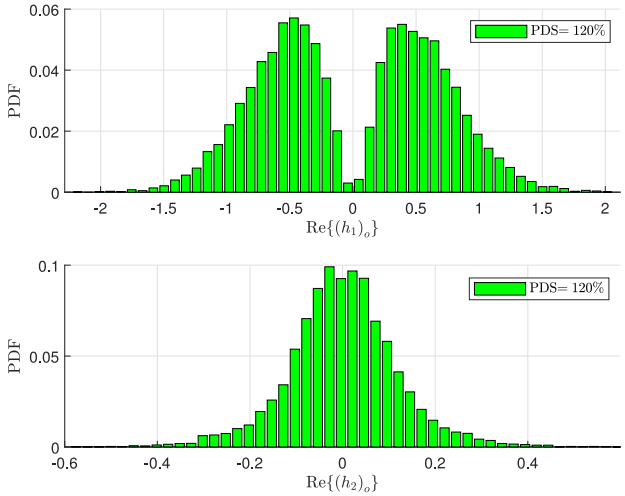

FIGURE 18. PDF of the real dimension of desired fading factors of a generalized mediumband channel (see (46)), where $\beta = 0.22$ and $N = 10$.

$r(t)$ in the absence of the noise can be modelled by:

$$r(t) = \sum_{v=1}^{L} \sqrt{E_s}(h_v)_o s\big(t - \hat{\tau} - (v-1)T_s\big) + \sqrt{E_s}\zeta_o u(t),$$

where $(h_v)_o$ for $v = 1, \ldots, L$ are the L optimum tap weights; and $\zeta_o u(t)$ is a complex uncorrelated interference signal, where $u(t)$ is a zero mean unit variance complex signal. The optimum tap weights are given by:

$$\boldsymbol{h} = \boldsymbol{W}^{-1}\boldsymbol{r}, \tag{52}$$

where $\boldsymbol{h} = \{(h_1)_o, \ldots, (h_L)_o\}^T$ is the $L \times 1$ complex tap weight vector and $\{.\}^T$ denotes the vector transpose operation. The $\boldsymbol{W} = \{w_{vl}\}$ is an $L \times L$ real matrix, of which the $(v,l)^{th}$ element is:

$$w_{vl} = R((v-l)T_s), \tag{53}$$

for $v, l = 1, \ldots, L$. Also, $\boldsymbol{r} = \{r_1, \ldots, r_l, \ldots, r_L\}^T$ is an $L \times 1$ complex vector with elements:

$$r_l = \sum_{n=0}^{N-1} \gamma_n R\big(\tau_n - \hat{\tau} - (l-1)T_s\big). \tag{54}$$

The fading parameter ζ_o can be found by extending the vth and lth indexes in (47) to L. The function $R(\tau)$ is given in (17) and $\gamma_n = \alpha_n e^{-j\phi_n}$ for $n = 0, \ldots, N-1$.

For notational simplicity, separate I/Q processing is omitted in Corollary 1. If the effect of separate I/Q synchronization is assumed, for the sake of completeness, we elaborate herein the revisions required to Corollary 1.

The r_l in (54), which is the lth element of $\boldsymbol{r}$, should be revised to:

$$r_l = \sum_{n=0}^{N-1} \mathrm{Re}\{\gamma_n\} R\big(\tau_n - \hat{\tau}_i - (l-1)T_s\big) + j\sum_{n=0}^{N-1} \mathrm{Im}\{\gamma_n\} R\big(\tau_n - \hat{\tau}_q - (l-1)T_s\big), \tag{55}$$

where $\hat{\tau}_i$ and $\hat{\tau}_q$ are respectively the time instances, which the I and Q branches of the RX synchronize to, as described in Section V. The corresponding fading parameters of the model mismatch error signal can be shown to be equal to (48), as

$$\zeta_o^i = \Bigg[\psi_0\Bigg(\sum_{v=1}^{L}\Big((h_v)_o^i\Big)^2 + \sum_{n=0}^{N-1}\mathrm{Re}\{\gamma_n\}^2\Bigg) + \sum_{n=0}^{N-1}\sum_{\substack{m=0\\m\neq n}}^{N-1}\mathrm{Re}\{\gamma_n\}\mathrm{Re}\{\gamma_m\}R(\tau_n - \tau_m) + \sum_{v=1}^{L}\sum_{\substack{l=1\\l\neq i}}^{L}(h_v)_o^i(h_l)_o^i R((v-l)T_s) - \sum_{v=1}^{L}\sum_{n=0}^{N-1} 2\mathrm{Re}\{\gamma_n\}(h_v)_o^i R\big(\tau_n - \hat{\tau}_i - (v-1)T_s\big)\Bigg]^{\frac{1}{2}}, \tag{48a}$$

$$\zeta_o^q = \Bigg[\psi_0\Bigg(\sum_{v=1}^{L}\Big((h_v)_o^q\Big)^2 + \sum_{n=0}^{N-1}\mathrm{Im}\{\gamma_n\}^2\Bigg) + \sum_{n=0}^{N-1}\sum_{\substack{m=0\\m\neq n}}^{N-1}\mathrm{Im}\{\gamma_n\}\mathrm{Im}\{\gamma_m\}R(\tau_n - \tau_m) + \sum_{v=1}^{L}\sum_{\substack{l=1\\l\neq i}}^{L}(h_v)_o^q(h_l)_o^q R((v-l)T_s) - \sum_{v=1}^{L}\sum_{n=0}^{N-1} 2\mathrm{Im}\{\gamma_n\}(h_v)_o^q R\big(\tau_n - \hat{\tau}_q - (v-1)T_s\big)\Bigg]^{\frac{1}{2}}. \tag{48b}$$

$$\begin{bmatrix} r_i(t) \\ r_q(t) \end{bmatrix} = \sqrt{E_s}\sum_{v=1}^{L}\begin{bmatrix} (h_v)_o^i s(t - \hat{\tau}_i - (v-1)T_s) \\ (h_v)_o^q s(t - \hat{\tau}_q - (v-1)T_s) \end{bmatrix} + \sqrt{E_s}\begin{bmatrix} \zeta_o^i u_i(t) \\ \zeta_o^q u_q(t) \end{bmatrix} \tag{49}$$

shown at the bottom of the previous page, where $(h_v)_o^i$ and $(h_v)_o^q$ are nothing but the real and imaginary parts of the vth optimum tap weight respectively. Consequently, in the presence of separate I/Q processing, the baseband equivalent received signal $r(t)$ in Corollary 1 in the absence of the noise can be elaborated as shown in (49), which is available at the bottom of the previous page.

VIII. IMPORTANT REMARKS

The results in this paper have wider implications. For instance, Theorem 1 and Corollary 1 can be made to be the basis of more realistic channel modelling. With a set of multipath profile measurements, Theorem 1 and Corollary 1 can be used to discretize measured data more realistically instead of dividing the excess delay axis into bins (or sampling grid) and assigning multipath components within these bins to a single tap as in [27, Sec. 3.4], [41] and [42, Ch. 6]. These models will automatically have optimum and more realistic tap weights along with more realistic statistical properties, which have been shown to be more important for wireless communication in Section VI. Also, they include the model mismatch error that is $\sqrt{E_s}\eta_o u(t)$ in Theorem 1 and $\sqrt{E_s}\zeta_o u(t)$ in Corollary 1 as a fully uncorrelated additive term, which may simplify further analysis greatly.

The analytical results in this paper are optimal in minimum-mean-squared-error sense and simple in the sense that they do not involve special functions, infinite series, or integrals and have a matrix formulation. Furthermore, the models herein could be made to be the basis of advanced interference-aware wireless networking technologies and more realistic performance analyses [43].

The analyses here show how exactly wireless propagation parameters (i.e., α_n, ϕ_n, τ_n) affect the channel models. For instance, Corollary 1 shows how exactly α_ns, ϕ_ns, τ_ns affect the tap weights and ζ_o in generalized mediumband channels. Using this additional knowledge, the effect of wireless propagation environment on the channel model (i.e., $(h_v)_o$s and ζ_o) could be altered by manipulating these underlying propagation parameters judiciously leading to more active wireless receiver architectures. It is clear that these wireless propagation parameters α_ns, ϕ_ns, τ_ns cannot be directly manipulated, but in some cases, new hybrid hardware transceiver architectures may exist that can indirectly manipulate these parameters [44].

IX. CONCLUSION

In this paper, a class of RF wireless channels that falls in the transitional region on the T_mT_s–plane between the narrowband and the broadband, named "***mediumband***" is studied. The effect of different propagation parameters (i.e., path delays, gains and phases) on the mediumband channels is analytically studied, and a new channel characterization in compact form was proposed, where the effects of transmit power, modulation, pulse shaping and fading have been captured in convenient forms. We further studied the effect of mediumband-ness on the I/Q processing and the bit error rate. Owing to its greater ability to reduce the deep fading, despite having significantly higher levels of ISI, mediumband systems have been shown to outperform narrowband systems over a large SNR region. The extent of the capability of mediumband systems to avoid deep fading was studied numerically. In addition to enabling more reliable and high-rate wireless communication, the analytical results and models herein may lead to more realistic channel modelling, and more advanced interference-aware networking and physical layer transceiver technologies for future wireless communication.

APPENDIX
PROOF OF THEOREM 1

Assuming $\hat{\tau}$ is the time that the RX is synchronized to, we consider the error signal defined by:

$$e(t) = r(t) - \sqrt{E_s}hs\big(t-\hat{\tau}\big). \tag{56}$$

The analysis herein is valid whether the symbol timing offset $\hat{\tau}$ in (56) is optimal or not. If $\hat{\tau}$ is optimal, the error signal would be weaker. It is otherwise, if $\hat{\tau}$ is not optimal. However, in the simulation studies throughout this paper, we use an exhaustive search method to find the optimum timing for $\hat{\tau}$. Consider the following conditional expectation:

$$J = \mathcal{E}\Big\{ |e(t)|^2 \Big| \Gamma, h \Big\}, \tag{57}$$

$$= \mathcal{E}\Big\{ \Big| r(t) - \sqrt{E_s}hs\big(t-\hat{\tau}\big) \Big|^2 \Big| \Gamma, h \Big\}, \tag{58}$$

where the expectation is taken with respect to the random process $s(t)$, but is conditioned on the propagation parameters, which is $\Gamma = \{\alpha_n, \phi_n, \tau_n\}$. This conditional expectation is the appropriate choice to characterize the behaviour of the channel for a given set of multipath components. The mean squared error J in (58) can be expanded and simplified

$$J = E_s\Bigg[|h|^2\mathcal{E}\Big\{s\big(t-\hat{\tau}\big)^2\Big\} + \sum_{n=0}^{N-1}|\gamma_n|^2\mathcal{E}\Big\{s(t-\tau_n)^2\Big\} + \sum_{n=0}^{N-1}\sum_{\substack{m=0\\m\neq n}}^{N-1}\gamma_n\gamma_m^*\mathcal{E}\{s(t-\tau_n)s(t-\tau_m)\} - \sum_{n=0}^{N-1}2\mathrm{Re}\big\{\gamma_n^* h\big\}\mathcal{E}\big\{s(t-\tau_n)s\big(t-\hat{\tau}\big)\big\}\Bigg]. \tag{59}$$

$$J = E_s\left[(1-0.25\beta)\left(|h|^2+\sum_{n=0}^{N-1}|\gamma_n|^2\right)+\sum_{n=0}^{N-1}\sum_{\substack{m=0\\m\neq n}}^{N-1}\gamma_n\gamma_m^* R(\tau_n-\tau_m)-\sum_{n=0}^{N-1}2\mathrm{Re}\{\gamma_n^* h\}R(\tau_n-\hat{\tau})\right]. \tag{62}$$

as shown in (59) as shown at the bottom of the page. The expectation $\mathcal{E}\{s(t-\tau_n)s(t-\tau_m)\}$ in (59) is the autocorrelation function of $s(t)$, which is a signal resulted from linear modulation. From [36, eq. (4-4-11)], the desired autocorrelation can be obtained as:

$$\mathcal{E}\{s(t)s(t+\tau)\} = \frac{1}{T_s}\sum_{q=-\infty}^{\infty}\psi_{ii}(q)\psi_{gg}(\tau-qT_s),$$

where $\psi_{ii}(q)$ is the autocorrelation of the real information sequence $\{I_k\}$, and $\psi_{gg}(\tau)$ is the time autocorrelation function of the raised cosine pulse $g(t)$. $\psi_{ii}(q)$ is defined as $\mathcal{E}_I\{I_k I_{k+q}\}$. In light of $\mathcal{E}\{|I_k|^2\}=1$, $\psi_{ii}(q)$ can be shown to be equal to:

$$\psi_{ii}(q) = \begin{cases} 1 & q=0 \\ 0, & \text{otherwise.} \end{cases} \tag{60}$$

Hence, $\mathcal{E}\{s(t)s(t+\tau)\} = \frac{1}{T_s}\psi_{gg}(\tau)$. Here the autocorrelation function $\psi_{gg}(\tau)$, which is defined as $\psi_{gg}(\tau)=\int_{-\infty}^{\infty} g(t)g(t+\tau)dt$, is well known. The desired result can thus be obtained as:

$$\mathcal{E}\{s(t)s(t+\tau)\} = R(\tau), \tag{61}$$

where $R(\tau)$ is given in (17). Applying the result in (61) into (59), J can be simplified to get (62). Due to the fact that the constellations are typically symmetric, $\mathcal{E}_I\{I_k\}=0$. Thus, the linear digital modulation (i.e., (5)) ensures that:

$$\mathcal{E}\{s(t)\} = 0. \tag{63}$$

So, the error process $e(t)$ is also a zero mean random process with variance J, which is given in (62).

A. OPTIMIZATION OF h

It is clear that J, which is quadratically dependent on h can further be optimized. Consider the following partial derivatives of J with respect to h:

$$\frac{\partial J}{\partial h^i} = \left(1-\frac{\beta}{4}\right)h^i - \sum_{n=0}^{N-1}\mathrm{Re}\{\gamma_n\}R(\tau_n-\hat{\tau}), \tag{64}$$

$$\frac{\partial J}{\partial h^q} = \left(1-\frac{\beta}{4}\right)h^q - \sum_{n=0}^{N-1}\mathrm{Im}\{\gamma_n\}R(\tau_n-\hat{\tau}). \tag{65}$$

where h^i and h^q denote the real and imaginary parts of h meaning $h = h^i + jh^q$. Equating these partial derivatives to zero, which is:

$$\frac{\partial J}{\partial h^i} = \frac{\partial J}{\partial h^q} = 0, \tag{66}$$

yields the optimum $h = h_o$, which is equal to:

$$h_o = \frac{\sum_{n=0}^{N-1}\gamma_n R(\tau_n-\hat{\tau})}{1-\frac{\beta}{4}}. \tag{67}$$

This completes the proof for h_o. Furthermore, by substituting the optimum value for h in (67) into (62), as shown at the top of the page, one can obtain the optimum error variance for the error process $e(t)$ as $E_s\eta_o^2$, where η_o is in (16). Consequently, in statistically equivalent form, $e(t)$ may be modelled by $e(t) = \sqrt{E_s}\eta_o u(t)$, where $u(t)$ is a zero mean, unit variance complex random process. In the absence of AWGN, $r(t)$ can thus be expressed as shown in (13) in Theorem 1.

ACKNOWLEDGMENT

Authors gratefully acknowledge the constructive comments of the anonymous reviewers and the associate editor, who handled the peer review of this paper.

REFERENCES

[1] ITU-ICT Data Analytics. "Global Connectivity Report 2022." 2022. [Online]. Available: https://www.itu.int/hub/publication/d-ind-global-01-2022
[2] M. Dangana, S. Ansari, S. M. Asad, S. Hussain, and M. A. Imran, "Towards the digital twin (DT) of narrow-band Internet of Things (NBIoT) wireless communication in industrial indoor environment," *Sensors*, vol. 22, no. 23, p. 9039, Nov. 2022.
[3] *Cisco Annual Internet Report (2018–2023)*, Cisco, San Jose, CA, USA, 2020.
[4] Z. Zhang et al., "6G wireless networks: Vision, requirements, architecture, and key technologies," *IEEE Veh. Technol. Mag.*, vol. 14, no. 3, pp. 28–41, Sep. 2019.
[5] G. L. Stuber, *Principals of Mobile Communications*, 2nd ed. New York, NY, USA: Kluwer, 2002.
[6] E. Tanghe et al., "The industrial indoor channel: Large-scale and temporal fading at 900, 2400, and 5200 MHz," *IEEE Trans. Wireless Commun.*, vol. 7, no. 7, pp. 2740–2751, Jul. 2008.
[7] W. H. Tranter et al., *The Best of the Best: Fifty Years of Communications and Networking Research*. Hoboken, NJ, USA: Wiley, Jan. 2007.
[8] G. R. MacCartney and T. S. Rappaport, "Millimeter-wave base station diversity for 5G coordinated multipoint (CoMP) applications," *IEEE Trans. Wireless Commun.*, vol. 18, no. 7, pp. 3395–3410, Jul. 2019.
[9] W. C. Jakes, *Microwave Mobile Communications*, 1st ed. New York, NY, USA: Wiley, 1975.
[10] Q. Li et al., "MIMO techniques in WiMAX and LTE: A feature overview," *IEEE Commun. Mag.*, vol. 48, no. 5, pp. 86–92, May 2010.
[11] M. Agiwal, A. Roy, and N. Saxena, "Next generation 5G wireless networks: A comprehensive survey," *IEEE Commun. Surveys Tuts.*, vol. 18, no. 3, pp. 1617–1655, 3rd Quart., 2016.
[12] *System Architecture for the 5G System, V.15*, 3GPP Standard TS 23.501, Dec. 2020.
[13] D. P. Taylor et al., "Wireless channel equalization," *Eur. Trans. Telecommun.*, vol. 9, no. 2, pp. 117–143, Mar./Apr. 1998.
[14] L. Wang, G. Liu, J. Xue, and K.-K. Wong, "Channel prediction using ordinary differential equations for MIMO systems," *IEEE Trans. Veh. Technol.*, vol. 72, no. 2, pp. 2111–2119, Feb. 2023.

[15] F. Mazzenga, "Channel estimation and equalization for M-QAM transmission with a hidden pilot sequence," *IEEE Trans. Broadcast.*, vol. 46, no. 2, pp. 170–176, Jun. 2000.
[16] J. Chuang, "The effects of time delay spread on portable radio communications channels with digital modulation," *IEEE J. Sel. Areas Commun.*, vol. SAC-5, no. 5, pp. 879–889, Jun. 1987.
[17] D. Tse and P. Viswanath, *Fundamentals of Wireless Communication*. Cambridge, U.K.: Cambridge Univ. Press, 2004.
[18] T. Kailath, "Correlation detection of signals perturbed by a random channel," *IRE Trans. Inf. Theory*, vol. 6, no. 3, pp. 361–366, Jun. 1960.
[19] Z. Ding *et al.*, "A survey on non-orthogonal multiple access for 5G: Research challenges and future trends," *IEEE J. Sel. Areas Commun.*, vol. 35, no. 10, pp. 2181–2195, Oct. 2017.
[20] V. R. Cadambe and S. A. Jafar, "Interference alignment and the degrees of freedom for the K user interference channel," *IEEE Trans. Inf. Theory*, vol. 54, no. 8, pp. 3425–3441, Aug. 2008.
[21] E. Telatar, "Capacity of multi-antenna Gaussian channels," *Eur. Trans. Commun.*, vol. 10, no. 6, pp. 585–595, Dec. 1999.
[22] S. M. Alamouti, "A simple transmitter diveristy scheme for wireless communications," *IEEE J. Sel. Areas Commun.*, vol. 16, no. 8, pp. 1451–1458, Oct. 1998.
[23] D. Greenwood and L. Hanzo, "Characterization of mobile radio channels," in *Mobile Radio Communications*, R. Steele, Ed. London, U.K.: Pentech, 1992, pp. 92–185.
[24] S. Haykin, "Cognitive radio: Brain-empowered wireless communications," *IEEE J. Sel. Areas Commun.*, vol. 23, no. 2, pp. 201–220, Feb. 2005.
[25] D. G. Sweeney and C. W. Bostian, "Implementing adaptive power control as a 30/20-GHz fade countermeasure," *IEEE Trans. Antennas Propag.*, vol. 47, no. 1, pp. 40–46, Jan. 1999.
[26] K. Cho and D. Yoon, "On the general BER expression of one and two-dimensional amplitude modulations," *IEEE Trans. Commun.*, vol. 50, no. 7, pp. 1074–1080, Jul. 2002.
[27] A. Goldsmith, *Wireless Communications*. Cambridge, U.K.: Cambridge Univ. Press, 2005.
[28] S. Sagari, W. Trappe, and L. Greenstein, "Equivalent tapped delay line channel responses with reduced taps," in *Proc. IEEE 78th Veh. Technol. Conf. (VTC Fall)*, Las Vegas, NV, USA, 2013, pp. 1–5.
[29] "Multipath propagation and parameterization of its characteristics," ITU, Geneva, Switzerland, ITU-Recommandation P.1407-8, 2021.
[30] H. Qiu et al., "Emulation of radio technologies for railways: A tapped-delay-line channel model for tunnels," *IEEE Access*, vol. 9, pp. 1512–1523, 2021.
[31] J. Kivinen, X. Zhao, and P. Vainikainen, "Empirical characterization of wideband indoor radio channel at 5.3 GHz," *IEEE Trans. Antennas Propag.*, vol. 49, no. 8, pp. 1192–1203, Aug. 2001.
[32] D. Cassioli, M. Z. Win, and A. F. Molisch, "The ultra-wide bandwidth indoor channel: From statistical model to simulations," *IEEE J. Sel. Areas Commun.*, vol. 20, no. 6, pp. 1247–1257, Aug. 2002.
[33] A. J. Coulson, "Maximum likelihood synchronization for OFDM using a pilot symbol: Algorithms," *IEEE J. Sel. Areas Commun.*, vol. 19, no. 12, pp. 2486–2494, Dec. 2001.
[34] D. A. Basnayaka, "Mediumband wireless communication," in *Proc. IEEE Veh. Technol. Conf.*, London, U.K., Sep. 2022.
[35] *Universal Mobile Telecommunications System; Radio Transmission and Reception, Version 3*, 3GPP Standard TS 25.102, 2000.
[36] J. G. Proakis, *Digital Communication*, 4th ed. New York, NY, USA: McGraw-Hill, 2000.
[37] M. Gans, "The effect of Gaussian error in maximal ratio combiners," *IEEE Trans. Commun. Technol.*, vol. CT-19, no. 4, pp. 492–500, Aug. 1971.
[38] G. J. Foschini and J. Salz, "Digital communications over fading radio channels," *Bell Syst. Tech. J.*, vol. 62, no. 2, pp. 429–456, Feb. 1983.
[39] S. Tang, P. Popovski, C. Zhang, and S. Obana, "Multi-slot over-the-air computation in fading channels," *IEEE Trans. Wireless Commun.*, early access, Feb. 22, 2023, doi: 10.1109/TWC.2023.3245304.
[40] B. Sklar, "Rayleigh fading channels in mobile digital communication systems. I. Characterization," *IEEE Commun. Mag.*, vol. 35, no. 7, pp. 90–100, Jul. 1997.
[41] G. L. Turin, "Introduction to spread-spectrum antimultipath techniques and their application to urban digital radio," *Proc. IEEE*, vol. 68, no. 3, pp. 328–353, Mar. 1980.
[42] A. F. Molisch, *Wireless Communications*, 2nd ed. Hoboken, NJ, USA: Wiley, 2011.
[43] I.-G. Lee and M. Kim, "IAPS: Interference aware power saving for high-efficiency wireless LANs in dense networks," *IEEE Commun. Lett.*, vol. 19, no. 12, pp. 2238–2241, Dec. 2015.
[44] T. Sun, J. Jia, and D. A. Basnayaka, "A wireless channel engineering method for future wireless communication," in *Proc. IEEE VTC-Spring*, 2023.

DUSHYANTHA A. BASNAYAKA (Senior Member, IEEE) received the B.Sc.Eng. (First-Class Hons.) and Ph.D. degrees in electrical engineering in 2006 and 2012, respectively. He is currently an Assistant Professor with Dublin City University, Dublin, Ireland. Prior to that, he was with the Institute for Digital Communication, The University of Edinburgh, U.K. In 2019, he was with the Division of Global Investments, Aberdeen Standard Investments, Edinburgh, U.K. He is an Editor of IEEE COMMUNICATIONS LETTERS.